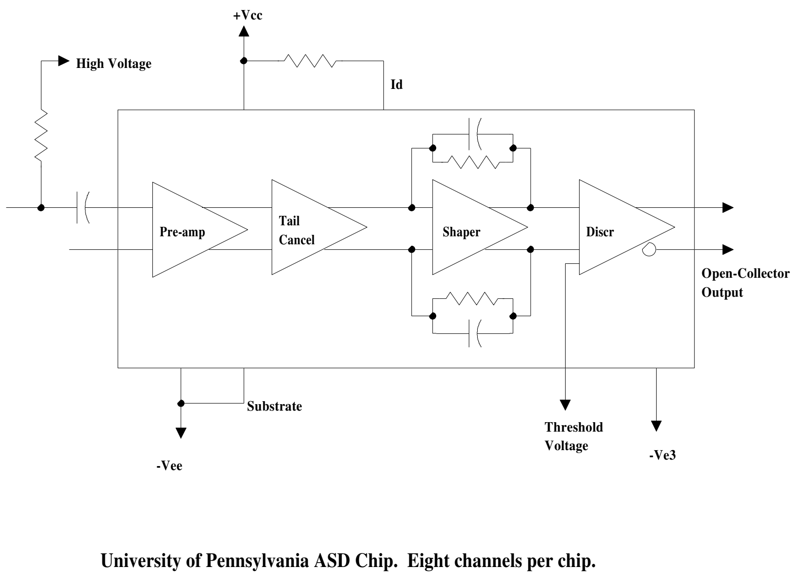

Figure 10.24: Block diagram of preamplifier-shaper-discriminator for the muon arm drift chambers.

chamber is thus a high priority task.

The drift-time measurement will be made using a TDC similar to the LeCroy MTD132A ASIC developed recently. This chip has a gray code scaler which may be driven by external clock at rates up to 125 MHz, together with an interpolation circuit which can measure arrival time to 1 ns. The design intrinsically has multihit capability. The present ASIC must be stopped in order to be read out, which does not mesh with the general Online philosophy adopted for PHENIX, as discussed in Chapter 11. A development effort to produce a data buffer which permits simultaneous read/write (to different locations) and which utilizes circular buffers is thus necessary. The same final TDC circuit will be used for the central drift chambers, so a single development effort will be pursued.

The muon identifier has modest requirements for both pulse height measurement and hit recording. A minimal circuit needs only a shaper plus discriminator, bit latch and buffer memory to allow for LVL-1 trigger latency. The amplitude of signals observed in the streamer tube tests indicates that little or no amplification is needed, although a fast shaper preceeding the discriminator is desireable. The discriminator outputs of three neighboring radial strips are "or"-ed together. The resulting 256 logical signals (32 per octant) for each plane of the muon identifier are sent to the LVL-1 Trigger circuits. If ongoing test beam measurements of a prototype muon identifier indicate that knowledge of the pulse height information aids in μ/π discrimination, a charge measurement will be made. This measurement needs be made with only 6–8-bit precision. A block diagram for the front-end electronics for the muon identifier is shown in Fig. 10.25.

Figure 10.25: Block diagram of front-end electronics for the muon identifier, including charge meaurement.

10.3.2 Trigger

The LVL-1 trigger decision for the muon arm uses the 3×256 logical signals from the muon identifier to count the number of muon candidates present in the muon arm. This sum is developed in a pipelined trigger processor for each beam crossing. The number of candidates is fed to the global LVL-1 trigger logic box, and the addresses of all candidate hits are stored in the trigger data stream for use in the LVL-2 trigger as masks for hits in the muon arm tracking chambers. A description of the LVL-1 trigger is given in Chapter 11.

The LVL-2 muon trigger computations use the output from LVL-1 together with the digitized hits from the three muon arm tracking stations. Each of the eight tracking octants has its own local trigger processor. The muon trigger data output from LVL-1 is one 32-bit word per octant, with each bit corresponding to a potential muon track in the muon identifier. This 32-bit word for each octant is smeared in the trigger processor by bit shifting and "or"ing to produce a mask for tracks at muon tracking station #3. The smearing is necessary in order to account for the range of incident angles of particles and for multiple scattering. Next, the station #3 chamber hits for the Y and Y' wires are unpacked and converted into another 32-bit word for each octant. This conversion also handles any needed alignment between station #3 and the muon identifier. The tracking stations do not have a projective radial readout geometry, so that a geometry conversion is necessary to match the readout pad geometry of the muon identifier. Similar 32-bit words for the two stereo planes may need to be prepared also. Finally, an "and" (or coincidence) is taken between these two words, producing a word containing potential muon hits for each octant of station #3.

This masked station #3 word is next used to mask station #2 hits exactly as the muon identifier is used to mask station #3. The result of this operation is then used to mask station #1, allowing for possible trajectories in the magnetic field. If the masked word from an octant of station #1 is not zero, then a potential muon track in that octant of the muon spectrometer is found. This procedure goes on in parallel for all eight octants. The resulting data can then be passed to a later processor in the LVL-2 trigger pipeline, or a decision could be taken at this step, should finding two candidate muon tracks proved to be a sufficiently selective trigger. Later stages of the LVL-2 trigger can apply invariant mass cuts.

10.4 Performance and Backgrounds

The simulations of the performance of the muon detector have been carried out independently and redundantly at one or more of Georgia State University, Los Alamos National Laboratory, Oak Ridge National Laboratory, the University of Tennessee and Vanderbilt University, using different methods and computer codes. This approach ensures a high degree of reliability and internal consistency in the results discussed below. In general PISA has formed the basis for all calculations except for certain simulations concerning signal-to-noise ratios, where faster and more simplified non-GEANT based codes were used.

Based on the design of the muon detector, the performance simulations have been split into four parts concerned with the performance of (1) the absorber, (2) the tracking and spectrometer performance, (3) the muon identifier, and (4) the integrated detector.

The discussion of the performance of the muon arm spectrometer is organized by increasing hit multiplicity. First, single track issues such as momentum resolution are discussed, followed by double track characteristics such as dimuon invariant mass resolution and acceptance estimates. Finally, multitrack characteristics, such as cell occupancy and track reconstruction, are presented.

10.4.1 Absorber

The steel pole tip of the central magnet is the main part of the hadron absorber for the muon arm. This steel pole tip is 60-cm thick (approximately 3.6λ) in the z direction, thus presenting from 61 cm to 75 cm of steel to the particles in the angular acceptance of the muon arm ($10° \leq \theta \leq 35°$). Simulation studies have shown that when this steel is integrated with the copper nosecone and the copper plug in front of the muon magnet piston, there is no particular advantage in tapering the downstream side of the central magnet pole, as shown in the present CM design. In the final CM design, this region will be left flat for reasons of simplicity and cost.

Simulations of particle leakage through various configurations of the magnet pole tip were performed using both GEANT 3.15, employing the GHEISHA and NUCRIN packages with 1 MeV tracking cuts, and with the LAHET (Los Alamos High Energy Transport) code system. The LAHET code system is a superset of the ORNL HETC code and incorporates EGS4, which provides detailed information on electron and photon leakage.

The central magnet and muon magnet steel geometries were taken from the design presented in Chapter 4. There is a copper nosecone in front of the pole tip of the central magnet, starting at 32 cm downstream of the nominal vertex to stay clear of the silicon pad inner detector array. The outer edge of the nosecone is along a ray joining the outer edge of the muon arm lampshade to a vertex 32 cm upstream of (i.e., farther away from the muon arm than) the nominal vertex, to ensure that any charged particle from the vertex that would enter the muon arm follows a trajectory through the face of the copper nosecone. The purpose of the nosecone is to reduce the flight path for hadrons from the collision point to the hadron absorber, which decreases the number of muons from weak decay entering the muon arm, as discussed in Section 10.4.4. It must be nonmagnetic so as not to perturb the central magnetic field.

A copper plug is placed immediately in front of the muon magnet piston to stop particles, particularly those from shower leakage, which otherwise might leave the central magnet pole at small polar angles and reach the tracking stations. It also provides additional absorber material for the more energetic primary particles at very forward angles which instead would strike the front face of the piston. Secondaries from such particles have a high probability of entering tracking stations #1 and #2. Early versions of this plug used tungsten in order to maximize the number of interaction lengths in the path of the highest energy hadrons. More recent studies show that copper provides nearly equivalent shielding capability at only 10% of the material cost of tungsten. This copper plug is 79.9-cm long, has a 40-cm deep recess for the beam-beam counters and has an outer tapered edge following a 10° line to match the muon magnet piston.

A 7-cm thick Pb "curtain" is placed at the downstream side of the central magnet steel to suppress photon and $e^{\pm}$ leakage, which are known from earlier studies with GEANT and LAHET to dominate the leakage from Fe or lower-Z absorber materials.

GEANT simulations were performed by tracking 100 GeV/A + 100 GeV/A central Au + Au events from the HIJET event generator through the muon absorber. The primary particles were produced at the nominal vertex, and all particles with $E_{kin} > 100$ MeV and $4.5° \leq \theta \leq 60.0°$ were followed. A tracking cut of $E_{kin} = 1.0$ MeV was used for all secondary tracks. The shower leakage into the muon arm was sampled at three locations (z = 180, 416, and 630 cm) corresponding to the position of the muon tracking stations. LAHET simulations were also performed with events from the HIJING event generator, which includes jet and mini-jet production in the initial phase of the collision and produces particles with harder p_T distributions than those obtained from HIJET or VENUS.

The results from GEANT simulations for the leakage of various shower products for different muon absorber geometries are summarized in Table 10.3 as the number of particles striking each of the three tracking stations in the muon arm. The addition of the copper piston plug plays an effective role in reducing the overall leakage into the acceptance of the muon arm, in some cases by as much as a factor of 10–15. Without the copper plug a sizable number of particles entering the chambers are secondaries from showers caused by particles hitting the piston part of the muon magnet directly; some of these secondaries backstream into the first tracking station.

The addition of the copper nosecone in front of the pole tip of the central magnet causes only a small (∼10–20%) decrease in the number of leakage particles (hadrons and leptons) with kinetic energies above 0.1 GeV reaching the tracking chambers. It does, however, reduce the number of decay muons (particularly muons above 1 GeV) originating from in flight decay in the free space before the hadron absorber. It also reduces the flux of energetic

Table 10.3: Comparison of shower leakage into the muon arm for various configurations of the muon absorber. The shower sampling was done at the locations corresponding to the three muon tracking stations. The numbers listed for the three energy bins are per Au + Au central event and are summed over the angular acceptance of the muon arm.

	Station #1			Station #2			Station #3		
Leakage Particle Type	<0.1 GeV	0.1-1.0 GeV	>1.0 GeV	<0.1 GeV	0.1-1.0 GeV	>1.0 GeV	<0.1 GeV	0.1-1.0 GeV	>1.0 GeV
	With Neither Cu Piston Plug nor Cu Nosecone								
γ	1208.2	20.2	0.0	1306.6	20.4	0.0	1219.2	19.2	0.0
e^+e^-	188.8	5.4	0.0	173.4	6.0	0.0	149.0	6.4	0.0
Charged Hadrons	15.8	67.4	10.6	10.6	63.4	12.0	7.8	56.6	11.8
$\mu^+\mu^-$	2.2	6.6	0.4	4.6	11.8	0.6	5.6	14.8	0.8
Neutral Hadrons	1165.6	81.2	3.4	834.8	83.2	3.8	747.6	77.6	3.8
Neutrons Only	1165.6	80.4	2.2	834.8	82.2	2.6	747.6	76.8	2.6
	With Cu Piston Plug but Without Cu Nosecone								
γ	256.6	2.4	0.0	135.6	1.8	0.2	116.0	1.4	0.2
e^+e^-	10.8	0.6	0.0	7.6	0.6	0.0	8.2	0.8	0.0
Charged Hadrons	4.4	26.2	7.0	2.4	19.6	6.4	2.4	17.6	5.6
$\mu^+\mu^-$	1.6	4.2	0.4	1.4	5.2	0.8	2.0	6.6	1.0
Neutral Hadrons	1040.4	69.0	2.0	662.6	50.4	2.0	603.0	46.6	2.0
Neutrons Only	1040.4	67.8	1.4	662.6	49.4	1.4	603.0	45.8	1.4
	With Both Cu Piston Plug and Cu Nosecone								
γ	232.4	1.8	0.0	132.0	1.6	0.0	116.4	1.6	0.2
e^+e^-	12.6	0.8	0.0	8.6	0.6	0.0	7.2	0.6	0.0
Charged Hadrons	6.6	23.0	4.8	3.6	14.6	4.8	2.8	13.6	4.2
$\mu^+\mu^-$	1.0	3.0	0.2	0.6	5.2	0.2	1.2	6.0	0.2
Neutral Hadrons	953.4	61.4	1.2	605.4	43.6	1.2	538.2	40.2	1.2
Neutrons Only	953.4	61.4	0.6	605.4	43.6	0.6	538.2	40.2	0.6

particles leaving the absorber, including sail-through hadrons and energetic shower particles, which can otherwise decay in flight *inside* the muon arm, producing additional decay muons. These muons are quite difficult to differentiate from muons coming from vector meson and virtual photon decays.

The kinetic energy spectra of the leakage particles arriving at tracking stations #1 and #3 as obtained from GEANT simulations are shown in Figs. 10.26 and 10.27. The p_T spectra of charged hadrons and $\mu^{\pm}$ reaching the first tracking station are shown in Fig. 10.28.

Most of the $e^{\pm}$ are below 20–30 MeV and do not pose any serious problem for the tracking chambers. The majority of the decay muons are below 200 MeV and will thus largely range out in the 30 cm of steel in front of the muon identifier. There is, however, about a 20%